

Mag-E4E: Trade Efficiency for Energy in Magnetic MIMO Wireless Power Transfer System

Xiang Cui^{*†}, Hao Zhou^{*†}, JiaLin Deng^{*†}, Wangqiu Zhou^{*†}, Xing Guo[‡], Yu Gu[§]

^{*}LINKE Lab, School of Computer Science and Technology, University of Science and Technology of China

[†]The CAS Key Laboratory of Wireless-Optical Communications, University of Science and Technology of China

[‡]School of Computer Science and Technology, Anhui university, China

[§]School of Computer and Information, Hefei university of Technology, China

Email: wondersu@mail.ustc.edu.cn, kitewind@ustc.edu.cn, {Jialind, rafazwq}@mail.ustc.edu.cn, 13040@ahu.edu.cn, yugu.bruc@ieee.org

Abstract—Magnetic resonant coupling (MRC) wireless power transfer (WPT) is a convenient and potential power supply solution for smart devices. The scheduling problem in the multiple-input multiple-output (MIMO) scenarios is essential to concentrate energy at the receiver (RX) side. Meanwhile, strong TX-RX coupling could ensure better power transfer efficiency (PTE), but may cause lower power delivered to load (PDL) when transmitter voltages are bounded. In this paper, we propose the frequency adjustment based PDL maximization scheme for MIMO MRC-WPT systems. We formulate such joint optimization problem and decouple it into two sub-problems, *i.e.*, high-level frequency adjustment and low-level voltage adaptation. We solve these two sub-problems with gradient descent based and alternating direction method of multipliers (ADMM) based algorithms, respectively. We further design an energy-voltage transform matrix algebra based estimation mechanism to reduce context measurement overhead. We prototype the proposed system, and conduct extensive experiments to evaluate its performance. As compared with the PTE maximization solutions, our system trades smaller efficiency for larger energy, *i.e.*, 361% PDL improvement with respect to 26% PTE losses when TX-RX distance is 10cm.

I. INTRODUCTION

In recent years, smart devices like mobile phones, smart-watches and tablets are becoming more and more popular. Meanwhile, device charging comes to be a recurring and significant issue. Wireless power transfer (WPT) has emerged as a promising solution to such issue. WPT systems could be realized by either inductive coupling (IC) or magnetic resonant coupling (MRC), in which the later utilizes electrical resonance to achieve higher efficiency and longer charging distance. Recently, beamforming technology has been imported to further support the multi-input and multi-output (MIMO) scenarios.

In the MIMO MRC-WPT systems, transmitter (TX) voltage scheduling is essential to guarantee that energy concentrate at receiver (RX) side. Extensive works have been proposed to express the scheduling target as maximizing the system power transfer efficiency (PTE) or its variations. The PTE upper bound is discussed with given power budget, and the existing conclusions imply that higher TX-RX coupling results in higher PTE [1], [2]. However, such results couldn't be ensured for power delivered to load (PDL) maximization in a practical MRC-WPT system where TX voltages are

often bounded. As shown in Fig. 1, strong TX-RX coupling is expected to achieve high PTE according to the conclusion in [1], but it will cause low PDL with bounded TX voltage. Such phenomenon could be explained as follows. In the view of TX circuit, the RX related equivalent impedance is not only decided by RX circuit itself, but also influenced by TX-RX coupling and system frequency. Therefore, stronger TX-RX coupling means larger RX equivalent impedance, which causes larger mismatching with TX internal impedance, and results in lower PDL according to maximum power transfer theorem [3].



(a) Strong TX-RX coupling results in high PDL
 (b) Tuning TX-RX coupling results in low PDL
 (c) Frequency adjustment for better PDL

Fig. 1. PDL evaluation in a MRC-WPT system with bounded TX voltage.

To relieve such impedance mismatching, we can either adjust TX-RX coupling or system frequency. Tuning for TX-RX coupling can be achieved through TX-RX distance adjustment as shown in Fig. 1(b), or specific designed TX coils [4]–[7], which may increase system implementation complexity. On the contrary, frequency adjustment is regarded as a more natural and efficient method, as shown in Fig. 1(c). For single-input single-output (SISO) MRC-WPT systems, frequency adjustment has been well studied [8]–[10]. The existing work have observed the frequency splitting phenomenon, *i.e.*, two PDL peaks form near the resonant frequency when TX-RX coupling is strong enough and TX voltage is bounded. However, frequency adjustment in MIMO scenarios hasn't been matured since the frequency-PDL relationship is more complicated than that in SISO scenarios.

In this paper, we investigate the scheduling problem in MIMO MRC-WPT system to maximize PDL by jointly considering frequency adjustment and TX voltage adaption. The difficulties of such problem come from the following

two aspects. The first one is due to the *joint optimization problem* itself. Even under fixed frequency, there still has no mature conclusion about the adaptation of TX voltage when they are restricted by given upper bound. The second difficulty is about the *context measurement overhead*. Solving the scheduling problem involves circuit context measurement, and some of them are variables under different frequencies, such as TX/RX impedances. Measuring such frequency-related context for each possible frequency will cause unaffordable cost.

In this paper, we address these challenges efficiently, and propose the frequency adjustment based PDL maximization system. Our work and contributions are summarized as follows.

- To the best of our knowledge, this is the first work to apply frequency adjustment for solving the impedance mismatching issue in practical MIMO MRC-WPT systems.
- We formulate the jointly frequency and TX voltage adaptation problem and decouple it into two sub-problems. The lower-level voltage adaptation sub-problem is solved with an alternating direction method of multipliers (ADMM) based algorithm. The upper-level frequency adjustment sub-problem is handled by gradient descent algorithm. Besides, we propose a matrix algebra based method to reduce the frequency-related context measurement overhead.
- We prototype the system and conduct extensive experiments to evaluate the performance. The results reveal that compared with the existing PTE maximization solutions, our solution could achieve 361% PDL improvement with respect to 26% PTE losses when TX-RX distance is 10cm. The improvement is more obvious when TX and RX are closely coupled.

II. RELATED WORK

A. Scheduling in MIMO MRC-WPT systems

The research about scheduling problem for MRC-WPT systems could be organized according to their optimization targets, *i.e.*, PTE optimization and PDL optimization.

1) *PTE Optimization*: The PTE optimization works are usually expressed as to maximize RX received power under the given total energy budget [1], [11]–[14].

Lang *et al.* formulated the MRC-WPT system with multiple TXs as a convex optimization problem and found the analytical result using Lagrangian duality theory [11]. Jadidian *et al.* designed MagMIMO [13], which could charge a phone at the distances of about 40cm independently of its orientation. Benjamin *et al.* utilized phased array to maximize power on one target while minimizing leakage fields in other locations [12]. Shi *et al.* designed MutiSpot [1], a wireless charger with multiple TX coils to charge all surrounding devices simultaneously at distances up to 50cm. Liu *et al.* proposed an optimization scheme to improve PTE by adjusting the amplitude of TX currents and the

RX resistances [4]. Zhou *et al.* incorporated MIMO MRC-WPT system with multiple relay components to extend the charging distance [14].

In summary, the PTE maximization problem of MIMO MRC-WPT system has been well studied. However, PTE maximization can't guarantee enough received power when with strong TX-RX coupling.

2) *PDL Optimization*: The PDL optimization works with limited voltage could be found in [2], [5], [6], [15]–[18], which can be cataloged into two kinds of work according to their optimization methods.

The first one is through *TX current scheduling* [2], [18], [19]. Yang *et al.* studied the magnetic beamforming problem in an MIMO MRC-WPT system to find all the boundary points [18]. Cao *et al.* proposed the requirement-driven scheduling method to maximize the sum of weighted received PDL of RXs [2]. Zhao *et al.* proposed a random method to achieve maximum received power with limited feedback information [19]. However, these works do not essentially solve the impedance mismatch.

The second kind is about *TX-RX coupling adjustment* [5]–[7], [15], [16]. Mohammad *et al.* proposed a RX load adjusting algorithm to relieve the over coupling [15]. Zhou *et al.* proposed a RX grouping and coupling tuning algorithm with special designed multilayer TX coils [6]. Moghadam *et al.* optimized the TX coil placement to maximize PDL over a given region [16]. Zhao *et al.* matched the impedance by selecting different capacitors [7]. Ghotbi *et al.* presented a specific designed 8-shaped TX coil structure [5]. These works adjust the RX equivalent impedance through various methods, including RX impedance adjusting, TX-RX distance adjusting and TX coils structure design. However, these works usually require special hardware structure, which results in high cost for implementation.

As we noticed, PDL related studies in MIMO MRC-WPT system are not mature enough. We prefer some more natural and low-cost solutions.

B. Frequency adjustment related research

Frequency is an important parameter in the MRC-WPT system. The influence of frequency to the system performance has been well studied in SISO scenarios.

The impact of frequency to PDL could be found in [8], [20], [21]. Ahn *et al.* proved that the resonant frequency does provide the best PTE, but it can't guarantee the maximum PDL [8]. Sample *et al.* further investigated the frequency splitting phenomenon where the MRC-WPC system wouldn't reach the maximum PDL at the resonant frequency but forms two peaks near it [21]. The research of Huang *et al.* demonstrated that the splitting is more obvious when RX is more tightly coupled with the TX [20].

Frequency adjustment has also been studied to enhance the performance of MRC-WPT systems [8]–[10], [17]. Niu *et al.* analyzed the frequency splitting phenomenon based on asymptotic coupled-mode theory [9]. Nam *et al.* proposed a frequency tracking scheme to maintain charging performance [10]. Ahn *et al.* suggested that the driving frequency

should be adjusted according to the coupling between TX and RX [8]. Dukju *et al.* provided the frequency conditions for PDL and PTE maximization in single-input multiple-output (SIMO) and multiple-input single-output (MISO) scenarios [17].

However, these solutions couldn't be directly generalized into the MIMO scenarios since the complicated PDL-frequency relationship in MIMO MRC-WPT systems.

III. PRELIMINARY

A. Application scenario

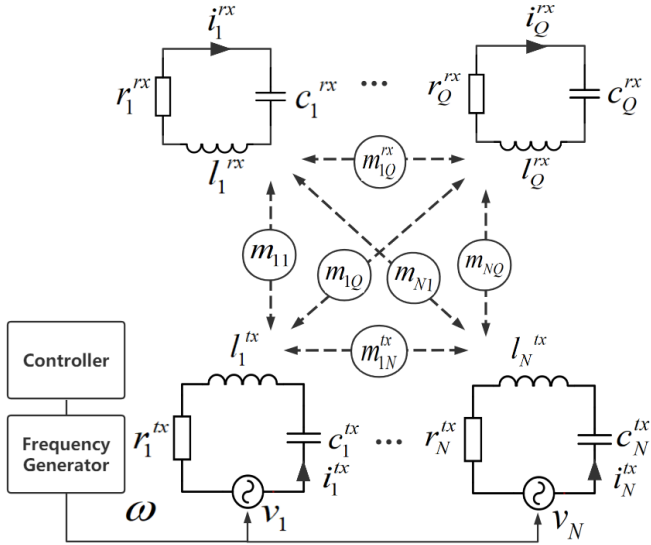


Fig. 2. Application scenario

Similar as the existing work [1], [2], [14], [18], our application scenario is shown in Fig. 2. The proposed MIMO MRC-WPT system consists of N TXs and Q RXs.

According to the circuit theory, the impedance under frequency ω could be expressed as $z_n^{tx}(\omega) = r_n^{tx} + j\omega l_n^{tx} + 1/j\omega c_n^{tx}$ for TX n , and $z_q^{rx}(\omega) = r_q^{rx} + j\omega l_q^{rx} + 1/j\omega c_q^{rx}$ for RX q . Here, r_n^{tx} (r_q^{rx}), l_n^{tx} (l_q^{rx}), c_n^{tx} (c_q^{rx}) denote the resistance, self-inductance and capacitor for TX n (RX q), respectively. Since our system are resonant based, we assume that each TX/RX has been tuned to resonant at the same frequency ω_0 , which means the impacts of self-inductance and capacitor cancel each other at ω_0 , *i.e.*, $z_n^{tx}(\omega_0) = r_n^{tx}$ and $z_q^{rx}(\omega_0) = r_q^{rx}$ for arbitrary TX n and RX q . Actually, even all the TX and RX aren't resonant at the same ω_0 , our algorithm could still work.

There are three types of mutual inductance in the MRC-WPT system, *i.e.*, TX-RX, TX-TX, and RX-RX ones. We denote m_{nq} for mutual inductance between TX n and RX q , $m_{n_1 n_2}^{tx}$ for TXs n_1 and n_2 , $m_{q_1 q_2}^{rx}$ for RXs q_1 and q_2 . In the proposed system, we assume that the TX-TX mutual inductance are already known since they could be measured offline. The other TX-RX and RX-RX mutual inductance could be obtained through the existing methods, such as that in [18] and [22]. In order to avoid RX coordination cost, we will introduce our solution without knowledge of concrete values for these RX-related terms in Sect. VI.

B. Circuit Equation

By applying Kirchoff's circuit law, we could express the circuit equations in matrix form as

$$\begin{cases} Z_R(\omega)\vec{i}_R = j\omega M \vec{i}_T, \\ j\omega M^\top \vec{i}_R + Z_T(\omega)\vec{i}_T = \vec{v}_T, \end{cases} \quad (1)$$

where the variables explanation are given in Table I, and the superscript (\top) denotes matrix transpose operation.

TABLE I
VARIABLES EXPLANATION

Term Definition	Explanation
$\vec{v}_T = [v_1, v_2, \dots, v_N]^\top$	TX voltages
$\vec{i}_T = [i_1^{rx}, i_2^{rx}, \dots, i_Q^{rx}]^\top$	TX currents
$\vec{i}_R = [i_1^{rx}, i_2^{rx}, \dots, i_Q^{rx}]^\top$	RX currents
$R_R = \text{diag}[r_1^{rx}, \dots, r_Q^{rx}]$	RX resistances
$Z_R(\omega) = \begin{bmatrix} z_1^{rx}(\omega) & j\omega m_{12}^{rx} & \cdots & j\omega m_{1Q}^{rx} \\ j\omega m_{21}^{rx} & z_2^{rx}(\omega) & \cdots & j\omega m_{2Q}^{rx} \\ \vdots & \vdots & \ddots & \vdots \\ j\omega m_{Q1}^{rx} & j\omega m_{Q2}^{rx} & \cdots & z_Q^{rx}(\omega) \end{bmatrix}$	RX impedance and RX-RX mutual inductance under frequency ω
$Z_T(\omega) = \begin{bmatrix} z_1^{tx}(\omega) & j\omega m_{12}^{tx} & \cdots & j\omega m_{1N}^{tx} \\ j\omega m_{21}^{tx} & z_2^{tx}(\omega) & \cdots & j\omega m_{2N}^{tx} \\ \vdots & \vdots & \ddots & \vdots \\ j\omega m_{N1}^{tx} & j\omega m_{N2}^{tx} & \cdots & z_N^{tx}(\omega) \end{bmatrix}$	TX impedance and TX-TX mutual inductance under frequency ω
$M = \begin{bmatrix} m_{11} & m_{21} & \cdots & m_{N1} \\ m_{12} & m_{22} & \cdots & m_{NN} \\ \vdots & \vdots & \ddots & \vdots \\ m_{1Q} & m_{2Q} & \cdots & m_{NQ} \end{bmatrix}$	TX-RX Mutual inductance

C. PDL Analysis

Our target is to maximize the PDL, *i.e.*, RX received power. For convenience of subsequent optimization process, we devise the expression of PDL in terms of TX voltages.

1) *TX current based expression:* The PDL of RX q is $|i_q^{rx}|^2 r_q^{rx}$. According to Eq.(1), we could express system PDL as

$$P(\omega) = \sum_{q=1}^Q |i_q^{rx}|^2 r_q^{rx} = \vec{i}_R^* R_R \vec{i}_R = \vec{i}_T^* H(\omega)^* R_R H(\omega) \vec{i}_T, \quad (2)$$

where the superscript (*) denotes the conjugate transpose operation. $H(\omega) \triangleq j\omega Z_R(\omega)^{-1} M$ is the transform matrix among TX currents and RX currents under frequency ω , *i.e.*, $\vec{i}_R = H(\omega) \vec{i}_T$.

2) *TX voltage based expression:* With simple matrix conversion, we could derive the relationship among \vec{v}_T and \vec{i}_T as

$$\begin{cases} \vec{v}_T = Y(\omega) \vec{i}_T, \\ Y(\omega) \triangleq Z_T(\omega) + B(\omega), \\ B(\omega) \triangleq \omega^2 M^\top Z_R^{-1}(\omega) M. \end{cases} \quad (3)$$

Then, we could express the sum of PDL based on TX voltages as

$$\begin{aligned} P &= \vec{i}_T^* H(\omega)^* R_R H(\omega) \vec{i}_T = \vec{i}_T^* \text{real}(B(\omega)) \vec{i}_T \\ &= \vec{v}_T^* (Y(\omega)^{-1})^* \text{real}(B(\omega)) Y(\omega)^{-1} \vec{v}_T = \vec{v}_T^* A(\omega) \vec{v}_T. \end{aligned} \quad (4)$$

where the function $\text{real}(\cdot)$ means the real part of a matrix.

Here, the second step in Eq. (4) is due to the theorem demonstrated in [1] which is $H(\omega)^*R_RH(\omega) = \text{real}(B(\omega))$. The third step is a simple substituting of Eq. (3) into Eq. (2). The last one is based on the definition of energy-voltage transform matrix $A(\omega) \triangleq (Y(\omega)^{-1})^* \text{real}(B(\omega))Y(\omega)^{-1}$.

The energy-voltage transform matrix $A(\omega)$ is essential for the proposed frequency and voltage adaptation problem. We regard it as already known matrix when solving the optimization problem, and we will introduce the matrix estimation method in Sect. VI to obtain $A(\omega)$ with reduced measurement overhead.

IV. PROBLEM OVERVIEW

In this section, we formulate our PDL maximization problem. Since it's a joint optimization problem, we decouple it into two sub-problems, along with an overview of our solution.

A. Problem formulation

1) *Optimization target*: Our optimization target is PDL, i.e., $\vec{v}_T^*A(\omega)\vec{v}_T$ according to Eq.(4).

2) *Optimization variable*: We regard TX voltages \vec{v}_T as the control variables like existing work [1], [2], [11]–[18]. Besides \vec{v}_T , we further consider adjustment of frequency ω in the optimization problem.

3) *Optimization constraint*: We assume the voltage of each TX is restrict by given upper bound, i.e., $|v_n|^2 \leq V_{\max}^2$ for each TX n , which is more meaningful for practical MRC-WPT systems than only consideration of power budget constraint.

As for now, we could formulate our frequency and voltage adaptation (FVA) problem as follows.

$$\text{FVA} = \max_{\{\vec{v}_T, \omega\}} \sum_{q=1}^Q |i_q^{rx}|^2 r_q^{rx} = \max_{\{\vec{v}_T, \omega\}} \vec{v}_T^* A(\omega) \vec{v}_T, \quad (5)$$

subject to

$$|v_n|^2 \leq V_{\max}^2, \quad \forall 1 \leq n \leq N, \quad (\text{C5a})$$

$$\omega_{\min} \leq \omega \leq \omega_{\max}, \quad (\text{C5b})$$

where Constraint (C5a) restricts the bound of voltage amplitude for each TX as V_{\max} . Constraint (C5b) states the valid range of frequency. Here, V_{\max} , ω_{\min} , and ω_{\max} are often decided according to hardware implementation.

B. Problem decoupling

The FVA problem (5) is obvious a joint optimization problem. Therefore, we could decouple it into two sub-problems for easier solution.

The low-level voltage adaption (VA) problem is to maximize PDL under given frequency, i.e.,

$$\text{VA}(\omega) = \max_{\{\vec{v}_T\}} \vec{v}_T^* A(\omega) \vec{v}_T, \quad \text{s.t. (C5a).} \quad (6)$$

The high-level frequency adjusting (FA) problem is to search for the optimal frequency based on the result of low-level sub-problem, which could be expressed as

$$\text{FA} = \max_{\{\omega\}} \text{VA}(\omega), \quad \text{s.t. (C5b).} \quad (7)$$

It's obvious that problem (7) is identical as the original problem (5).

C. Solution overview

As for the low-level voltage adaptation problem, we will introduce an ADMM-based algorithm in the next section to solve it effectively.

As for the high-level frequency adjusting sub-problem, it belongs a search problem with a single variable ω over a continuous derivation function $\text{VA}(\omega)$. Thus, it could be efficiently solved by the classic gradient descent methods.

Meanwhile, although we regard the energy-voltage transform matrix $A(\omega)$ as already known constants when solving the VA sub-problem, we will introduce the RX-independent mechanism to measure the matrix in Sect. VI-B, along with the matrix algebra based method to further reduce the measurement overhead in Sect. VI-C.

V. ADMM-BASED SOLUTION FOR VOLTAGE ADAPTION SUB-PROBLEM

In this section, we discuss our solution for low-level voltage adaptation sub-problem under fixed frequency. For easier expression, we omit the notation of ω in this section.

The problem (6) belongs to a standard semi-definite programming (SDP) problem. The problem could be solved by existing toolkit, such as CVX [23]. However, CVX-based solution requires a large amount of iterations to obtain a feasible approximation solution in the randomization process. Due to the real-time optimization requirement, we convert the problem to a general form consensus problem and efficiently solve it with an ADMM-based algorithm.

A. Consensus optimization problem

The general form consensus problem has been discuss in [24], [25], which is in the form of

$$\max_{\{x_i, z\}} \sum_{i=1}^N f_i(x_i), \quad \text{s.t. } x_i = \tilde{z}_i, \quad \forall 1 \leq i \leq N. \quad (8)$$

The problem has global variable z and local variables x_i . The objective of the problem $\sum_{i=1}^N f_i(x_i)$ is separable in the local variables x_i .

Each of the local variables consists of a selection of the components of the global variables, i.e., $\Omega(x_i) \subseteq \Omega(z)$ for each x_i where $\Omega(\cdot)$ is the set of components in the variable. We denote $z[e]$ as the value of the component e in the global variable z , and $x_i[e]$ as that in the local variable x_i . Then, we have $\tilde{z}_i = \{z[e] | e \in \Omega(x_i)\}$. Intuitively, \tilde{z}_i is the global variables' view of what the local variable x_i should be.

B. Problem conversion

1) *Objective separation:* The objective of the consensus optimization problem can be view as the sum of multiple local functions. Then our first step is to convert the optimization objective $\vec{v}_T^* A \vec{v}_T$ into the sum form.

The $N \times N$ matrix A is obvious a Hermitian matrix, i.e., $A^* = A$. Therefore, it has N non-negative real-number eigenvalues ($\lambda_i, 1 \leq i \leq N$) along with the corresponding unit eigenvectors ($\vec{\gamma}_i, 1 \leq i \leq N$). For arbitrary vector \vec{v}_T , it can be expressed as the linear addition of these eigenvectors, i.e., $\vec{v}_T = \sum_{i=1}^N \alpha_i \vec{\gamma}_i$ where each coefficient factor α_i is a complex number. Thus, we conclude that

$$\begin{aligned} \vec{v}_T^* A \vec{v}_T &= \sum_{i=1}^N \alpha_i^* \vec{\gamma}_i^* \sum_{j=1}^N A \alpha_j \vec{\gamma}_j = \sum_{i=1}^N \alpha_i^* \vec{\gamma}_i^* \sum_{j=1}^N \lambda_j \alpha_j \vec{\gamma}_j \\ &= \sum_{i=1}^N \lambda_i \alpha_i^* \alpha_i. \end{aligned} \quad (9)$$

The second step in Eq.(9) is due to the definition of eigenvector, i.e., $A \vec{\gamma}_i = \lambda_i \vec{\gamma}_i$. The third one is because the unit eigenvectors are orthogonal to the others, i.e., $\vec{\gamma}_i^* \vec{\gamma}_j$ equals one only when $i = j$, and zero otherwise.

As for now, the objective of our problem has been converted into the form as addition of multiple terms. The optimization variables have changed from \vec{v}_T to the linear coefficient factors (α_i) of the eigenvectors.

2) *Voltage constraint conversion:* When treat coefficient factors as optimization variables, we have $v_n = \sum_{i=1}^N \gamma_{i,n} \alpha_i$ where $\gamma_{i,n}$ is the n-th element in vector $\vec{\gamma}_i$.

For voltage constraint $|v_n|^2 \leq V_{\max}^2$ of TX n , we could view it as N separated regulation functions for different α_i . To be specific, we define regulation functions as follows.

$$\begin{cases} g_{n,i}(z, x_{n,i}) = \begin{cases} 0, & \text{if } |v_{n,i}(z, x_{n,i})|^2 \leq V_{\max}^2, \\ -\infty, & \text{otherwise.} \end{cases} \\ v_{n,i}(z, x_{n,i}) = \sum_{j \neq i}^N \gamma_{j,n} z_j + \gamma_{i,n} x_{n,i}, \end{cases} \quad (10)$$

where $v_{n,i}(z, x_{n,i})$ denotes the voltage of TX n . The value of coefficient factor α_i is specialized by local variable $x_{n,i}$, and the values for other factors are given by global variable $z = [z_1, \dots, z_N]$.

The regulation function $g_{n,i}(z, x_{n,i})$ denotes the TX n 's voltage constraint in the view of coefficient factor α_i .

3) *Consensus problem conversion:* Let's define the local function as

$$f_{n,i}(z, x_{n,i}) = \lambda_i |x_{n,i}|^2 + g_{n,i}(z, x_{n,i}). \quad (11)$$

Then, our voltage adaptation problem (6) could be written as a general consensus problem, i.e.,

$$\text{VA-Consensus} = \max_{\{z, x_{n,i}\}} \sum_{n=1}^N \sum_{i=1}^N \frac{1}{N} f_{n,i}(z, x_{n,i}), \quad (12)$$

subject to

$$x_{n,i} = \tilde{z}_i, \quad \forall 1 \leq n \leq N, 1 \leq i \leq N. \quad (\text{C12a})$$

It is obvious that the VA-Consensus problem (12) is identical to the original VA problem (6).

C. ADMM-Based Algorithm

According to [26], the augmented Lagrangian of the VA-Consensus problem is

$$\begin{aligned} L_\rho(x_{n,i}, y_{n,i}, z) &= \sum_{n=1}^N \sum_{i=1}^N \frac{1}{N} (f_{n,i}(z, x_{n,i})) \\ &\quad - \text{real}(y_{n,i}(x_{n,i} - \tilde{z}_i)) - (\rho/2) \|x_{n,i} - \tilde{z}_i\|_2^2, \end{aligned} \quad (13)$$

with penalty parameter $\rho > 0$ and dual variable $y_{n,i}$. $\|\cdot\|_2$ is the Euclidean norm.

The resulting ADMM-based algorithm consists of the iterations as follows.

1) *X update step:* The update step for $x_{n,i}$ is

$$\begin{aligned} x_{n,i}^{k+1} &= \operatorname{argmax}_{\frac{1}{N} f_{n,i}(z^k, x_{n,i})} \\ &\quad - \text{real}(y_{n,i}^k(x_{n,i} - \tilde{z}_i^k)) - (\rho/2) \|x_{n,i} - \tilde{z}_i^k\|_2^2. \end{aligned} \quad (14)$$

It could be regarded as to maximize the quadratic function of variable $x_{n,i}$, under the convex searching space constrained by regulation function $g_{n,i}$. Such single variable optimization problem could be easily solved by the existing optimizer.

2) *Z update step:* Z update step could be expressed as

$$\tilde{z}_i^{k+1} = \operatorname{argmax}_{\{z_i\}} \sum_{n=1}^N \left(y_{n,i}^k \tilde{z}_i - (\rho/2) \|x_{n,i}^{k+1} - \tilde{z}_i\|_2^2 \right). \quad (15)$$

We could further derive the following equation to ease calculation, and we omit the derivation process due to the lack of space.

$$\tilde{z}_i^{k+1} = \frac{1}{N} \sum_{n=1}^N (x_{n,i}^{k+1} + y_{n,i}^k / \rho). \quad (16)$$

3) *Y update step:* The update step for $y_{n,i}$ is straightforward as

$$y_{n,i}^{k+1} = y_{n,i}^k + \rho (x_{n,i}^{k+1} - \tilde{z}_i^{k+1}). \quad (17)$$

VI. HIGH-LEVEL SOLUTION AND ESTIMATION OF MATRIX $A(\omega)$

In this section, we first discuss our solution for high-level frequency adjusting sub-problem. Then we introduce the details about how to estimate the energy-voltage transform matrix $A(\omega)$.

A. Gradient descent based solution for frequency adjusting sub-problem

The high-level frequency adjusting sub-problem FA belongs a search problem with a single variable ω over a continuous derivation function $VA(\omega)$. Due to the simplicity of the problem, we use mature first-order optimization algorithms to solve this problem. Specifically, we choose gradient descent algorithm to search for the optimal frequency.

Furthermore, we use multi-starts strategies to avoid getting trapped in a local optimum [27]. According to the experiment results, we set the number of starts as five to achieve a good trade-off between accuracy and computational complexity.

During the process for solving the high-level FA problem, we need to call the low-level voltage adaption $VA(\omega)$ subproblem multiple times with different frequencies. Each time when $VA(\omega)$ is called, we need to prepare the energy-voltage transform matrix $A(\omega)$ in advance. In the following subsections, we will introduce how to obtain these matrices.

B. RX-independent $A(\omega)$ measurement with given ω

We can notice the RX-related terms exist in the matrix $A(\omega)$, such as TX-RX/RX-RX mutual inductance, and RX impedance. These terms could be derived through the existing solutions, such as the magnetic MIMO channel estimation methods in [18] and [22]. However, such derivation process involves cooperation or feedback communication from the RXs, which increases the RX implementation complexity.

On the other hand, we only need $A(\omega)$ to solve the VA problem other than the concrete values of the RX-related terms. The definition of the energy-voltage transform matrix is given as $A(\omega) \triangleq (Y(\omega)^{-1})^* \text{real}(B(\omega)) Y(\omega)^{-1}$, with $Y(\omega) \triangleq Z_T(\omega) + B(\omega)$. We assume matrix $Z_T(\omega)$ is already known since it can be measured offline. Then, we only need to obtain $B(\omega)$ to calculate $A(\omega)$.

According to the TX current-voltage relationship in Eq. (3), we apply a specific TX voltage setting, and perform current measurement at TX side to obtain one observation which brings N equations for the unknown $N \times N$ matrix $B(\omega)$. Thus, N orthogonal observations is enough to solve $B(\omega)$. After that, we could easily obtain $A(\omega)$ based on its definition.

Here, we obtain $A(\omega)$ from observations at TX side without cooperation of RXs, which is a RX-independent measurement based method.

C. Matrix algebra based $A(\omega)$ estimation for arbitrary ω

1) *Basic idea:* We could perform RX-independent measurement to obtain $A(\omega)$ for any frequency. However, there will exist unacceptable overhead if we need to perform measurement for each possible frequency when solve the high-level FA problem. We need a more efficient scheme to reduce such measurement overhead. According to the definition, $A(\omega)$ is decided by $B(\omega) \triangleq M^T Z_R(\omega)^{-1} M$. Therefore, our intuition is to analyze the relationship among matrix $B(\omega)$ with different frequency and try to derive the matrix for new frequency from known ones.

2) *Derivation for MISO scenarios:* Let us consider the scenario with only one RX q . Since the RX resonates in frequency ω_0 , we have $j\omega_0 l_q^{rx} + 1/j\omega_0 c_q^{rx} = 0$.

With arbitrary factor α , we could conduct the RX impedance under the frequency ω_0 , $\alpha\omega_0$ and $\frac{1}{\alpha}\omega_0$ as follows.

$$\begin{cases} z_q^{rx}(\omega_0) = r_q^{rx}, \\ z_q^{rx}(\alpha\omega_0) = r_q^{rx} + j(\alpha - \frac{1}{\alpha})\omega_0 l_q^{rx}, \\ z_q^{rx}(\frac{1}{\alpha}\omega_0) = r_q^{rx} - j(\alpha - \frac{1}{\alpha})\omega_0 l_q^{rx}. \end{cases} \quad (18)$$

Then, the corresponding matrix $B_q(\omega)$ could be expressed as

$$\begin{cases} B_q(\omega_0) = M_q^\top M_q \frac{1}{r_q^{rx}}, \\ B_q(\alpha\omega_0) = M_q^\top M_q \frac{r_q^{rx} - j(\alpha - \frac{1}{\alpha})\omega_0 l_q^{rx}}{r_q^{rx2} + (\alpha - \frac{1}{\alpha})^2 \omega_0^2 l_q^{rx2}}, \\ B_q(\frac{1}{\alpha}\omega_0) = M_q^\top M_q \frac{r_q^{rx} + j(\alpha - \frac{1}{\alpha})\omega_0 l_q^{rx}}{r_q^{rx2} + (\alpha - \frac{1}{\alpha})^2 \omega_0^2 l_q^{rx2}}, \end{cases} \quad (19)$$

where M_q is a $N \times 1$ vector for TX-RX mutual inductance related to RX q . We can further derive that

$$\begin{cases} B_q(\alpha\omega_0) + B_q(\frac{1}{\alpha}\omega_0) = M_q^\top M_q \frac{2r_q^{rx}}{r_q^{rx2} + (\alpha - \frac{1}{\alpha})^2 \omega_0^2 l_q^{rx2}}, \\ B_q(\alpha\omega_0) - B_q(\frac{1}{\alpha}\omega_0) = M_q^\top M_q \frac{-2j(\alpha - \frac{1}{\alpha})\omega_0 l_q^{rx}}{r_q^{rx2} + (\alpha - \frac{1}{\alpha})^2 \omega_0^2 l_q^{rx2}}. \end{cases} \quad (20)$$

By comparing two terms in Eq. (20), we could eliminate the term of $M_q^\top M_q$ and obtain the ratio of $\omega_0 l_q^{rx}$ to r_q^{rx} recorded as follows.

$$\sigma = \frac{\omega_0 l_q^{rx}}{r_q^{rx}} = j \left(\frac{\alpha}{\alpha^2 - 1} \right) \frac{B_q(\alpha\omega_0) - B_q(\frac{1}{\alpha}\omega_0)}{B_q(\alpha\omega_0) + B_q(\frac{1}{\alpha}\omega_0)}. \quad (21)$$

As for now, when facing another new frequency as $\beta\omega_0$, we can easily obtain its corresponding $B_q(\beta\omega_0)$ with known $B_q(\omega_0)$ and σ as

$$B_q(\beta\omega_0) = B_q(\omega_0) \frac{1 - j(\beta - \frac{1}{\beta})\sigma}{1 + (\beta - \frac{1}{\beta})^2 \sigma^2}. \quad (22)$$

According to our derivation process, we should firstly perform three measurement processes for $B_q(\omega)$ at frequency ω_0 , $\alpha\omega_0$, $\frac{1}{\alpha}\omega_0$, respectively. Then, we could estimate $B_q(\omega)$ for any given frequency.

3) *Extension to MIMO scenarios:* When multiple RXs exist, matrix $B(\omega)$ is more complicated due to the existence of mutual inductance between RXs. However, RX-RX mutual inductance is much smaller than others due to the smaller size of RX coils and deployment diversities of RXs [14]. Therefore, we could ignore RX-RX mutual inductance, and have the following equations about $B(\omega)$.

$$\begin{aligned} B(\omega) &= M^\top Z_R^{-1} M = M^\top \text{diag}([\frac{1}{z_1^{rx}(\omega)}, \dots, \frac{1}{z_Q^{rx}(\omega)}]) M \\ &= \sum_{q=1}^Q M_q^\top \frac{1}{z_q^{rx}(\omega)} M_q = \sum_{q=1}^Q B_q(\omega). \end{aligned} \quad (23)$$

The matrix algebra based Eq. (23) suggests that once $B_q(\omega)$ are derived through the aforementioned mechanism, $B(\omega)$ could be estimated, and so as well for the energy-voltage transform matrix $A(\omega)$.

4) *Further discussion:* The first issue is about the number of need measurement for matrix estimation. It is obvious that three matrix measurement processes should be conducted for each RX q , i.e., for frequencies ω_0 , $\alpha\omega_0$ and $\frac{1}{\alpha}\omega_0$. Therefore, total $3 \times Q$ matrix measurement should be performed.

The second issue is about the implementation of measurement processes for $B_q(\omega)$. It should be performed in the state with only RX q turned on, and the other RXs are turned off. Such state could be achieved through a simple RX coordination mechanism. For example, we could broadcast signals to let all the RXs response randomly to turn on or off. The above coordination mechanism has been added to our prototype.

The third issue is about the error caused by RX-RX mutual inductance ignorance. Since the results of Eq. (23) is close, but not equal to actual $B(\omega)$, we could adopt a simple compensation method to deal with it. In other words, we first solve the high-level frequency adjustment problem based on the estimated $A(\omega)$ to obtain a candidate frequency. After that, we further perform compensation searching near the candidate frequency, which is based on the measured $A(\omega)$ as introduced in Sect. VI-B.

VII. PROTOTYPE IMPLEMENTATION

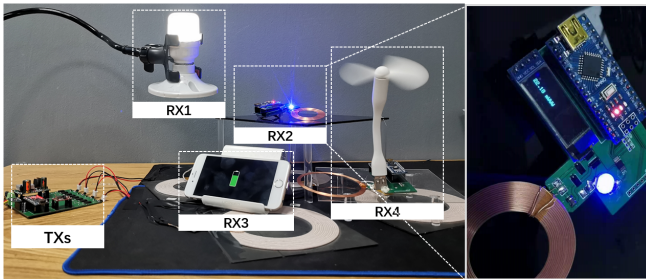


Fig. 3. Prototype testbed.

We build a prototype testbed for our system as shown in Fig. 3. The resonant frequency is set as $1.0MHz$, which is within the frequency range of common wireless charging systems [28]. Note that our solution is independent of the resonant frequency, i.e., our algorithm could also work with other resonant frequency, such as $6.78MHz$ which is the frequency adopted in Rezence [29].

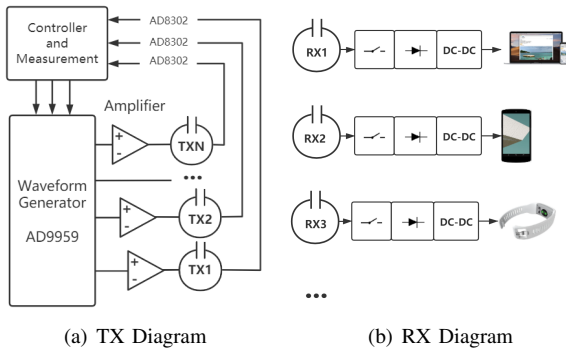


Fig. 4. Prototype Architecture

A. TX implementation

The architecture of the TX is illustrated in Fig. 4(a), which consists of TX coils, amplifier, frequency synthesizer, controller and measurement. Our transmitter is composed of four copper coils resonating with their own serial capacitors. Each TX coil area is $0.015m^2$, which is powered by sinusoidal signal amplified by an ADA4870 [30] amplifier chip. The amplifier is able to provide a maximum TX voltage up to 20 volts. The primary signal is generated by direct digital synthesizer (DDS) chip AD9959 which can output signals with frequency from $100khz$ to $100Mhz$ with $0.12Hz$ frequency tuning step [31]. We use Arduino for TX digital logic. For matrix $A(\omega)$ measurement, we adopt oscilloscope to measure energy-voltage transform matrix, and the results are transmitted to controller.

B. RX implementation

The architecture of RX is illustrated in Fig. 4(b). The RX circuit can be matched with coils of different sizes. We use the copper coil with area of about $0.002m^2$ and thickness of about $1.0mm$. As introduced in Sect. VI-C, we need to decode the TX broadcast command to achieve the state with only one RX turned on. To realize such function, each RX is equipped with a MCU to decode the TX broadcast, along with switch circuit to achieve the on-off control which is similar as that in Qi specification [32]. Furthermore, we add a power monitor at each RX to record the received PDL.

VIII. EVALUATION

In this section, extensive experiments are conducted to evaluate the proposed system.

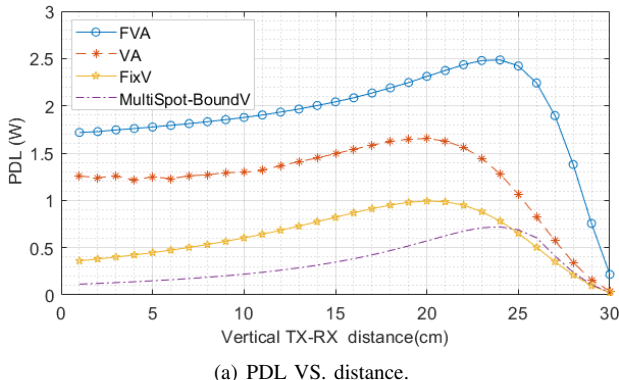
A. Macro evaluation

1) *Experiment setup:* We perform experiments on the prototype. The resonant frequency is $1MHz$, and the valid frequency ranges from $0.9MHz$ to $1.1MHz$. The upper bound of TX voltage is set as $5V$ for evaluation. We choose different kind of RX payload in experiments, including LED, motor and lithium battery.

Our prototype includes four TXs. After fixing the locations of TXs, we evaluate the proposed system with varied RX numbers and TX-RX distance.

We compare the proposed system, denoted as FVA, with the other three solutions. The first solution only performs voltage adaptation, denoted as VA. The second FixV solution always sets voltage as the upper bound for each TX without any adjustment. The third one is the PTE maximization algorithm in MultiSpot system [1], denoted as MultiSpot-BoundV, where the optimization results are scaled to ensure voltage bound constraints. Noted that all the other solutions work at the resonant frequency without consideration of frequency adjustment.

2) *Influence of TX-RX distance:* We place two RXs on a horizontal plane which keeps parallel with the TX plane, and vary the vertical distance between these two planes. Fig. 5(a) plots the PDL with varied distance. Our solution outperforms the other three solutions with an average improvement of



(a) PDL VS. distance.

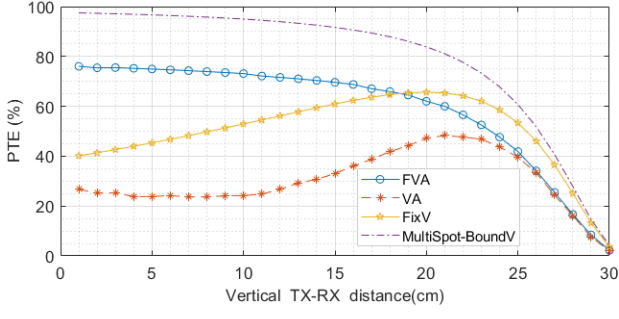


Fig. 5. Influence of TX-RX distance.

58%, 310% and 461%, respectively. The results demonstrate the effectiveness of the proposed system, especially when TX-RX are closely coupled, *e.g.*, when TX-RX distance is within 10cm.

Fig. 5(b) plots the corresponding PTE. As expected, MultiSpot-BoundV achieves the best PTE. We could notice that our system tends to sacrifice PTE for better PDL. For example, FVA trades 26% PTE loss for 361% PDL improvement as compared with Multispot-BoundV when TX-RX distance is 10cm.

We should further notice that the effective charging distance of Multispot-BoundV is about 30cm in our experiment which is different as the results of 50cm in [1]. That is because our working voltage amplitude is limited as 5V.

3) Influence of RX number: We fix the vertical TX-RX distance as 10cm and 25cm, and vary the number of RXs from 1 to 6 to evaluate the scalability of the proposed system. Figs. 6(a) and 6(b) illustrate the total achieved PDL of all RXs. As shown in the figure, the total PDL gradually increases and stabilizes with increased RX number. For example, PDL increases from 0.8W (single RX) to 2.3W (5 RXs) when TX-RX distance is 25cm. That is because more RX coils would cover a larger area, thereby picking up more magnetic flux. In all cases, our solution could achieve the best PDL, *i.e.*, average improvements of 100.4%, 304% and 325% over the other three solutions, respectively.

4) Influence of RX orientation: We further evaluate the RX orientation influence. As shown in Fig. 7(a), we put two RXs with three TXs and fix the vertical TX-RX distance as about 15cm. Both RX coils are placed horizontally at first. Then we gradually rotate one of RXs from horizontal to vertical while keeping another one stable.

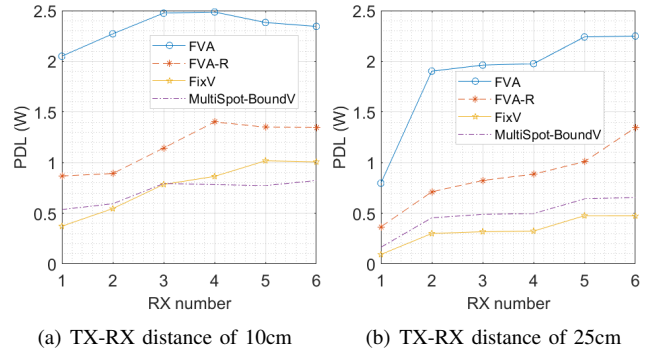
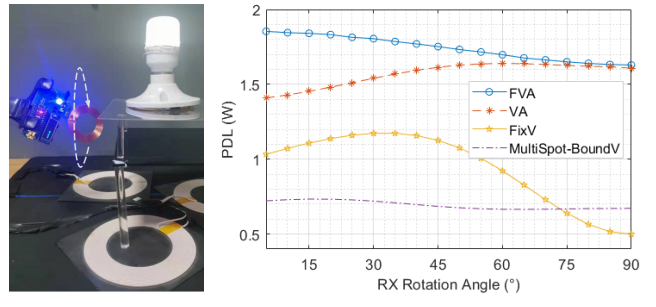


Fig. 6. Influence for RX number.

Fig. 7(b) plots the performance with different orientation angles. The X-axis represents the angle between the RX coil and the horizontal plane. The average PDL improvements of FVA to the other solutions are 10.9%, 85.1% and 151.1%, respectively. The results demonstrate that our proposed system is robust to RX orientation.

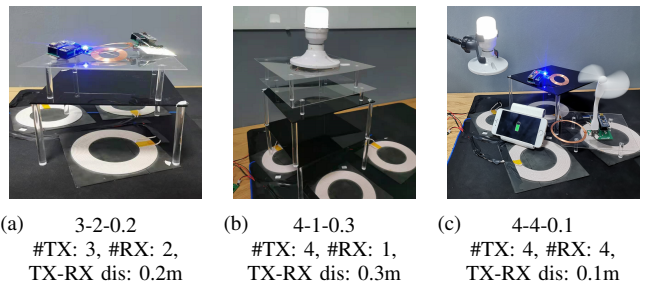


(b) Achieved PDL

Fig. 7. Influence of RX orientation.

B. Micro evaluation

In this subsection we evaluate our system under different scenarios. For better illustration, we take three typical deployments, for example, which is shown in Fig. 8. Here, ‘3-2-0.2’ denotes the scenario with 3 TXs, 2 RXs, and the average vertical TX-RX distance as 0.2m.



(a) 3-2-0.2 (b) 4-1-0.3 (c) 4-4-0.1
#TX: 3, #RX: 2, #TX: 4, #RX: 1, #TX: 4, #RX: 4,
TX-RX dis: 0.2m TX-RX dis: 0.3m TX-RX dis: 0.1m

#TX: 3, #RX: 2, #TX: 4, #RX: 1, #TX: 4, #RX: 4,
TX-RX dis: 0.2m TX-RX dis: 0.3m TX-RX dis: 0.1m

#TX: 3, #RX: 2, #TX: 4, #RX: 1, #TX: 4, #RX: 4,
TX-RX dis: 0.2m TX-RX dis: 0.3m TX-RX dis: 0.1m

#TX: 3, #RX: 2, #TX: 4, #RX: 1, #TX: 4, #RX: 4,
TX-RX dis: 0.2m TX-RX dis: 0.3m TX-RX dis: 0.1m

#TX: 3, #RX: 2, #TX: 4, #RX: 1, #TX: 4, #RX: 4,
TX-RX dis: 0.2m TX-RX dis: 0.3m TX-RX dis: 0.1m

#TX: 3, #RX: 2, #TX: 4, #RX: 1, #TX: 4, #RX: 4,
TX-RX dis: 0.2m TX-RX dis: 0.3m TX-RX dis: 0.1m

#TX: 3, #RX: 2, #TX: 4, #RX: 1, #TX: 4, #RX: 4,
TX-RX dis: 0.2m TX-RX dis: 0.3m TX-RX dis: 0.1m

#TX: 3, #RX: 2, #TX: 4, #RX: 1, #TX: 4, #RX: 4,
TX-RX dis: 0.2m TX-RX dis: 0.3m TX-RX dis: 0.1m

1) Low-level solution evaluation: We adopt ADMM-based algorithm to solve the low-level $VA(\omega)$ sub-problem. Fig. 9(a) illustrates the evaluation of the proposed algorithm under different application scenarios at the resonant frequency. We record performance of two other solutions in the same scenarios for comparison. The first one is gradient descent, marked as GD. The second one adopts the widely used CVX toolkit for voltage adaptation problem [23].

As shown in Fig. 9(a), we could notice that ADMM achieves similar performance as CVX, and both of them outperform GD with an average improvement of 15%. On the other hand, our ADMM based algorithm tends to converge within tens of iterations as shown in Fig. 9(b), which outperforms CVX solution which normally requires more than 4000 iterations [2].

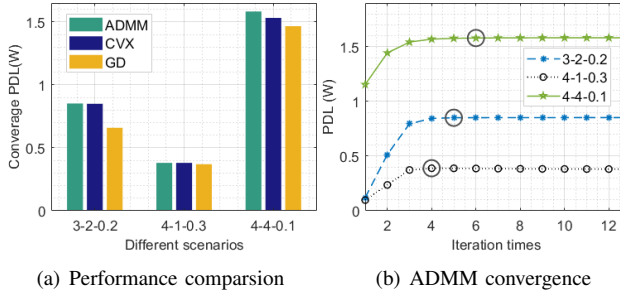


Fig. 9. Low-level solution evaluation.

2) *High-level solution evaluation:* For high-level frequency adjustment problem, we use gradient descent with five starts to search for the optimal frequency. We compare our method with three other solutions. The Greedy method performs greedy search near the resonant frequency ω_0 . The two Brute-force methods scan the valid range of frequency with different number of sampling frequencies, *i.e.*, 1000 and 2000 points.

Fig. 10(a) illustrates the achieved PDL, and Fig. 10(b) plots the number of function calls to the low-level voltage adaption problem, which is used as the metric to evaluate computational complexity.

Our solution achieves similar PDL as the two Brute-force methods with differences less than 1.5%. However, the function call times in our solution is only 20.6% as compare to Brute-force 1000 method. The results suggest that our algorithm has a good balance between accuracy and computational complexity.

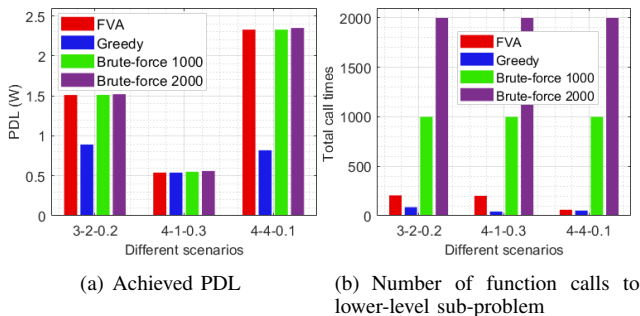


Fig. 10. Evaluation for high-level solution.

3) $A(\omega)$ estimation evaluation: As discussed in Sect. VI. In order to balance the computation cost and accuracy, our high-level solution is implemented as search for candidate frequency based on the estimated $A(\omega)$ in the first round, and then perform compensation searching near the candidate frequency based on the measured $A(\omega)$ in the second round.

We compare our algorithm with the other two solutions here. The first one, denoted as FVA-WOComp, is similar

as ours but without the compensation searching round. The second one, denoted as Measure-Only, only uses measured $A(\omega)$ for high-level solution.

Fig. 11(a) plots the achieved PDL, and Fig. 11(b) plots the number of needed measurement. The results demonstrate that our matrix estimation method could dramatically reduce the amount of measurements by more than 88.3% as compared with Measure-Only, and the second round compensation searching could well tackle the error caused by RX-RX mutual inductance ignorance in the estimation process with an average 2.9% improvement as compared with FVA-WOComp.

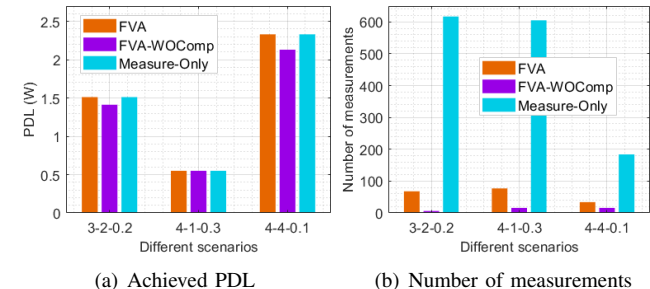


Fig. 11. Evaluation for matrix estimation mechanism.

IX. CONCLUSION

In this paper, we investigated the scheduling problem in MIMO MRC-WPT systems where TX voltages are bounded. We formulated the PDL maximization problem as a joint optimization problem for both frequency adjustment and voltage adaptation.

We decoupled the joint optimization problem and solved the two sub-problems with the ADMM based and gradient descent based algorithms. We further introduced the matrix algebra based mechanism to estimate the energy-voltage transform matrix for saving measurement overhead. Extensive experiments were conducted over the prototype. As compared with the existing PTE maximization solutions, our solution could achieve 361% PDL improvement with respect to 26% PTE losses when TX-RX distance is 10cm.

In the future, we will combine our work with other TX-RX coupling adjustment methods, such as TX coil selection and TX-RX distance adjustment, to further enhance the PDL in MIMO MRC-WPT systems.

X. ACKNOWLEDGEMENT

The research is partially supported by National Key RD Program of China 2019YFB2102200, China National Funds for Distinguished Young Scientists with No. 61625205, China National Natural Science Foundation with No. 61832010, 62172379, 61772488, 61751211, 61520106007, and 62132018, Key Research Program of Frontier Sciences, CAS. No. QYZDY-SSW-JSC002, University Synergy Innovation Program of Anhui Province with No. GXXT-2019-024. The authors would like to thank Information Science Laboratory Center of USTC for the hardware services. Hao Zhou and Xing Guo are the corresponding authors.

REFERENCES

- [1] L. Shi, Z. Kabelac, D. Katabi, and D. Perreault, "Wireless power hotspot that charges all of your devices," in *Proceedings of the 21st Annual International Conference on Mobile Computing and Networking*, 2015, pp. 2–13.
- [2] G. Cao, H. Zhou, H. Zhang, J. Xu, P. Yang, and X.-Y. Li, "Requirement-driven magnetic beamforming for mimo wireless power transfer optimization," in *2018 15th Annual IEEE International Conference on Sensing, Communication, and Networking (SECON)*. IEEE, 2018, pp. 1–9.
- [3] C. Kong, "A general maximum power transfer theorem," *IEEE Transactions on Education*, vol. 38, no. 3, pp. 296–298, 1995.
- [4] X. Liu, B. Mei, X. Wang, and Z. Wen, "Magnetic transceiver beamforming for a 2×2 magnetic resonance charging system," *IEEE Journal of Electromagnetics, RF and Microwaves in Medicine and Biology*, vol. 2, no. 3, pp. 186–192, 2018.
- [5] I. Ghotbi, M. Najjarzadegan, H. Sarfaraz, S. J. Ashtiani, and O. Shoaei, "Enhanced power-delivered-to-load through planar multiple-harmonic wireless power transmission," *IEEE Transactions on Circuits and Systems II: Express Briefs*, vol. 65, no. 9, pp. 1219–1223, 2018.
- [6] W. Zhou, H. Zhou, W. Hua, F. Zhou, and X. Cui, "Imp: Impedance matching enhanced power-delivered-to-load optimization for magnetic mimo wireless power transfer system," in *2021 IEEE/ACM 29th International Symposium on Quality of Service (IWQoS)(IWQoS 2021)*, 2021, pp. 1–10.
- [7] Y. Zhao, X. Li, C.-Z. Xu, and Y. Ji, "Smart multi-coil-based magnetic resonance prototype for wireless power transfer," in *2018 IEEE Wireless Power Transfer Conference (WPTC)*. IEEE, 2018, pp. 1–4.
- [8] D. Ahn and S. Hong, "Effect of coupling between multiple transmitters or multiple receivers on wireless power transfer," *IEEE Transactions on Industrial Electronics*, vol. 60, no. 7, pp. 2602–2613, 2013.
- [9] W. Q. Niu, W. Gu, J. Chu, and A. Shen, "Coupled-mode analysis of frequency splitting phenomena in cpt systems," *Electronics letters*, vol. 48, no. 12, pp. 723–724, 2012.
- [10] N. Y. Kim, K. Y. Kim, and C.-W. Kim, "Automated frequency tracking system for efficient mid-range magnetic resonance wireless power transfer," *Microwave and Optical Technology Letters*, vol. 54, no. 6, pp. 1423–1426, 2012.
- [11] H.-D. Lang, A. Ludwig, and C. D. Sarris, "Convex optimization of wireless power transfer systems with multiple transmitters," *IEEE Transactions on Antennas and Propagation*, vol. 62, no. 9, pp. 4623–4636, 2014.
- [12] B. H. Waters, B. J. Mahoney, V. Ranganathan, and J. R. Smith, "Power delivery and leakage field control using an adaptive phased array wireless power system," *IEEE Transactions on Power Electronics*, vol. 30, no. 11, pp. 6298–6309, 2015.
- [13] J. Javidian and D. Katabi, "Magnetic mimo: How to charge your phone in your pocket," in *Proceedings of the 20th annual international conference on Mobile computing and networking*, 2014, pp. 495–506.
- [14] H. Zhou, W. Hua, J. Deng, X. Cui, X.-Y. Li, and P. Yang, "Joint power routing and current scheduling in multi-relay magnetic mimo wpt system," in *IEEE INFOCOM 2020-IEEE Conference on Computer Communications*. IEEE, 2020, pp. 1–9.
- [15] M. R. V. Moghadam and R. Zhang, "Multiuser wireless power transfer via magnetic resonant coupling: performance analysis, charging control, and power region characterization," *IEEE Transactions on Signal and Information Processing over Networks*, vol. 2, no. 1, pp. 72–83, 2015.
- [16] ———, "Node placement and distributed magnetic beamforming optimization for wireless power transfer," *IEEE Transactions on Signal and Information Processing over Networks*, 2017.
- [17] D. Ahn and S. Hong, "Effect of coupling between multiple transmitters or multiple receivers on wireless power transfer," *IEEE Transactions on Industrial Electronics*, vol. 60, no. 7, pp. 2602–2613, 2013.
- [18] G. Yang, M. R. V. Moghadam, and R. Zhang, "Magnetic mimo signal processing and optimization for wireless power transfer," *IEEE Transactions on Signal Processing*, vol. 65, no. 11, pp. 2860–2874, 2017.
- [19] Y. Zhao, X. Li, C.-Z. Xu, and Y. Ji, "Random beamforming for multi-coil magnetic resonance wireless power transfer system," in *2018 IEEE Wireless Power Transfer Conference (WPTC)*. IEEE, 2018, pp. 1–4.
- [20] R. Huang, B. Zhang, D. Qiu, and Y. Zhang, "Frequency splitting phenomena of magnetic resonant coupling wireless power transfer," *IEEE Transactions on Magnetics*, vol. 50, no. 11, pp. 1–4, 2014.
- [21] A. P. Sample, D. T. Meyer, and J. R. Smith, "Analysis, experimental results, and range adaptation of magnetically coupled resonators for wireless power transfer," *IEEE Transactions on industrial electronics*, vol. 58, no. 2, pp. 544–554, 2010.
- [22] W. Hua, X. Cui, H. Zhou, P. Yang, and X. Li, "Parallel feedback communications for magnetic mimo wireless power transfer system," in *2019 16th Annual IEEE International Conference on Sensing, Communication, and Networking (SECON)*, 2019, pp. 1–9.
- [23] M. Grant and S. Boyd, "Cvx: Matlab software for disciplined convex programming, version 2.1," 2014.
- [24] S. Boyd, N. Parikh, and E. Chu, *Distributed optimization and statistical learning via the alternating direction method of multipliers*. Now Publishers Inc, 2011.
- [25] H. Zhou, Y. Ji, X. Wang, and S. Yamada, "eicic configuration algorithm with service scalability in heterogeneous cellular networks," *IEEE/ACM Transactions on Networking*, vol. 25, no. 1, pp. 520–535, 2016.
- [26] L. Li, X. Wang, and G. Wang, "Alternating direction method of multipliers for separable convex optimization of real functions in complex variables," *Mathematical Problems in Engineering*, vol. 2015, 2015.
- [27] A. György and L. Kocsis, "Efficient multi-start strategies for local search algorithms," *Journal of Artificial Intelligence Research*, vol. 41, pp. 407–444, 2011.
- [28] F. Carobolante, "Wireless power transfer, overcoming the technological hurdles," *APEC. IEEE*, 2014.
- [29] R. Tseng, B. von Novak, S. Shevde, and K. A. Grajski, "Introduction to the alliance for wireless power loosely-coupled wireless power transfer system specification version 1.0," in *Wireless Power Transfer (WPT), 2013 IEEE*. IEEE, 2013, pp. 79–83.
- [30] Analog Devices. ADA4870 High Speed, High Voltage, 1 A Output Drive Amplifier. [Online]. Available: <https://www.analog.com/en/products/ada4870.html>
- [31] ———. AD9959 4 Channel 500 MSPS DDS with 10-bit DACs. [Online]. Available: <https://www.analog.com/en/products/ad9959.html>
- [32] Wireless Power Consortium. (2010) System Description Wireless Power Transfer, Vol. 1, v1.2.3. [Online]. Available: http://www.y-adagio.com/public/committees/iec_tc100ags/meetings/29/100ags_438.pdf